Research Article Vol. 3, No. 6 / 15 June 2020 / OSA Continuum 1608
OSA CONTINUUM

Upper bound of efficiency for Smith-Purcell emission and evanescent-to-propagating wave conversion in metal-groove metasurfaces

NINGXIAO JIANG, YANAN SONG, JIAYUAN DU, XINYU ZHAO, XIAODONG SUN, AND XINHUA HU*

Department of Materials Science, and Key Laboratory of Micro- and Nano-Photonic Structures (Ministry of Education), and Laboratory of Advanced Materials, Fudan University, Shanghai 200433, China
*huxh@fudan.edu.cn

Abstract: When a charged particle moves parallel and close to the surface of a metasurface, intense Smith-Purcell radiation can be observed at resonant frequencies. Here, we present a systematic investigation on the Smith-Purcell radiation and evanescent-to-propagating wave conversion in metal-groove metasurfaces. Based on a coupled mode theory, analytic formulas are derived for the resonant frequency, Q-factor, and wave conversion efficiency at resonant frequency. The accuracy of the formulas is verified by numerical simulations. It is found that the resonant frequency and Q-factor depend on the depth and filling ratio of the grooves, respectively. A high Q-factor can be obtained by decreasing the filling ratio of the grooves. As the Q-factor increases, the wave conversion efficiency at resonant frequency increase but exhibits an upper limit. Such an upper bound of efficiency ($C_{r,max} = 4$) can be approached at a moderate Q-factor ($Q = 16$) or an optimal filling ratio of the grooves ($f_s = 0.05$). Our results may benefit the construction of compact high-power free-electron light sources.

1. Introduction

In 1953, Smith and Purcell demonstrated that when a charged particle moves parallel and close to the surface of a metallic diffraction grating, it can drive the grating to emit electromagnetic (EM) radiation [1]. Unlike traditional Cherenkov effect [2], such Smith-Purcell emission can occur even at a particle velocity much lower than the light speed in vacuum. Hence, this phenomenon is easier to observe, which forms the basis of many significant applications including radiation generators and particle detectors [3–10].

Metasurfaces are a novel class of two-dimensional EM materials, enabling fascinating EM properties and functionalities [11–19]. Unlike common diffraction gratings, metasurfaces are composed of EM subwavelength resonator arrays. It has been recently discovered that at resonant frequencies, metasurfaces can exhibit higher efficiency in producing Smith-Purcell emission than traditional gratings [20–31]. In particular, using metasurfaces of periodic metallic groove arrays, unidirectional Smith-Purcell emission can be efficiently generated above the metasurfaces [8,30,31]. High-intensity fields are located in the vacuum region rather than the metallic part of the metasurfaces, enabling high power output of radiations. For such resonant Smith-Purcell emission [21,22], a fundamental picture is that the evanescent waves bounded to swift charged particles can be converted into propagating waves more efficiently by the metasurfaces. However, a comprehensive investigation has not been presented on the relationship between the wave conversion efficiency and structural parameters for the metal-groove metasurfaces.

In this paper, we systematically study the Smith-Purcell radiation and evanescent-to-propagating wave conversion in metal-groove metasurfaces. Based on a coupling mode theory, we can derive analytic formulas for the resonant frequency, Q-factor, and evanescent-to-propagating wave conversion efficiency. The accuracy of formulas is verified by finite-element simulations. It is

#391540 https://doi.org/10.1364/OSAC.391540
Journal © 2020 Received 28 Feb 2020; revised 26 May 2020; accepted 2 Jun 2020; published 8 Jun 2020

OSA CONTINUUM

found that the resonant frequency and Q-factor of the metasurfaces are related to the depth and width of grooves, respectively. For ideal metal-groove metasurfaces, the Q-factor increases with decreasing the filling ratio of grooves. As the Q-factor increases, the wave conversion efficiency increases at resonant frequency but possesses an upper bound. Such an upper limit of efficiency ($C_{r,max} = 4$) can be approached at a moderate Q-factor ($Q = 16$) or an appropriate filling ratio of grooves ($f_s = 0.05$).

2. Theory

The metasurface under study is a metallic slab with a periodic groove array at its upper surface, as shown in Fig. 1(a). The metasurface is located at vacuum and its upper surface is at $z = 0$. The grooves have a period p and width Δ in the x direction, and a depth h in the z direction.

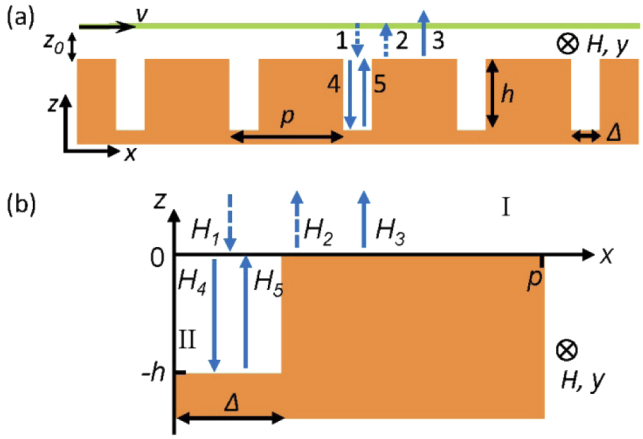

Fig. 1. (a) Schematic of the Smith-Purcell emission from a metal-groove metasurface consisting of a metallic slab with a periodic groove array. The grooves have a period of p, depth of h, and width of Δ. The metasurface is in the x-y plane and the grooves are along the y direction. Above and close to the metasurface, a uniform sheet of charged particles moves with a velocity v along the x direction. Consequently, evanescent waves 1 and 2, and propagating waves 3, 4, and 5 can occur in the system, with magnetic fields along the y direction. (b) A unit cell for the metasurface in (a).

At $z = z_0$ (above the metasurface) exists an uniform sheet of charged particles, which has a line charge density q in the y direction and moves with a velocity v along the x direction. The corresponding current density can be written as $\overline{J} = \int_0^{+\infty} \hat{x} I_0 \delta(z - z_0) \exp(ik_{x1}x - i\omega t) d\omega$, where $I_0 = q/2\pi$, $k_{x1} = \omega/v$, $\omega = 2\pi f$ is the angular frequency, and f is the frequency [22,23]. Hence, evanescent wave 1 can be generated below the swift charged particles. Its magnetic field is along the y direction and can be expressed as $\overline{H} = \int_0^{+\infty} H_1 \exp(ik_{x1}x + ik_{z1}z - i\omega t) d\omega$, where $H_1 = I_0 \exp(-ik_{z1}z_0)/2$ is the H-field with frequency f at $z = 0$, $k_{z1} = -i\sqrt{k_{x1}^2 - k_0^2}$, $k_0 = \omega/c$, and c is the light velocity in vacuum.

Due to the periodicity of the metasurface [see Fig. 1(b)], the H-field with frequency f in the region I ($0 < z < b$) can be approximately written as

$$H_I = H_1 \exp(ik_{x1}x + ik_{z1}z) + H_2 \exp(ik_{x1}x - ik_{z1}z) + H_3 \exp(ik_{x3}x + ik_{z3}z), \quad (1)$$

where the first term represents the incident evanescent wave 1, the second term relates to the reflected evanescent wave 2 (i.e., the zeroth-order diffraction), and the third term is for the propagating wave 3 (i.e., the -1st order diffraction) with $k_{x3} = k_{x1} - 2\pi/p$ and $k_{z3} = \sqrt{k_0^2 - k_{x3}^2}$.

OSA CONTINUUM

Diffracted waves with other orders are very evanescent and will slightly affect the results [see Figs. 3 and 4]. The H-field inside the metal groove [see Fig. 1(b)] can be approximately expressed as

$$H_{II} = H_4 \exp(ik_{z4}z) + H_5 \exp(-ik_{z4}z) \tag{2}$$

where the first and second terms denote the downward and upward propagating waves 4 and 5, respectively, and $k_{z4} = -k_0$. Higher-ordered waves with form of $\exp(ik_{z4}z)\cos(k_{x4}x)$ (where $k_{z4} = \sqrt{k_0^2 - k_{x4}^2}$, $k_{x4} = j\pi/\Delta$, $j = 1, 2, 3\ldots$) can also occur in the grooves. However, for long wavelengths with $\lambda > 2\Delta$, such waves become evanescent ($k_{x4} > k_0$ and thus k_{z4} is imaginary) and thus is neglected here.

For a unit cell of the metasurface (see Fig. 1(b)), the linking conditions at $z = 0$ are

$$H_I = H_{II} \text{ for } 0<x<\Delta, \tag{3}$$

$$\frac{\partial}{\partial z}H_I = \begin{cases} \frac{\partial}{\partial z}H_{II} \text{ for } 0<x<\Delta \\ 0 \text{ for } \Delta<x<p \end{cases}. \tag{4}$$

Multiplying Eq. (3) by $\int_0^\Delta dx$, Eq. (4) by $\int_0^p \exp(-ik_{x1}x)dx$, and Eq. (4) by $\int_0^p \exp(-ik_{x3}x)dx$ we have

$$b_1(H_1 + H_2) + b_2H_3 = H_4 + H_5, \tag{5}$$

$$b_3(H_1 - H_2) = H_4 - H_5, \tag{6}$$

$$b_4H_3 = H_4 - H_5, \tag{7}$$

where $b_1 = \Delta^{-1}\int_0^\Delta exp(ik_{x1}x)dx$, $b_2 = \Delta^{-1}\int_0^\Delta exp(ik_{x3}x)dx$, $b_3 = k_{z1}p/[k_{z4}\int_0^\Delta exp(-ik_{x1}x)dx]$, and $b_4 = k_{z3}p/[k_{z4}\int_0^\Delta exp(-ik_{x3}x)dx]$. Due to the total reflection at the bottom of the metallic groove, we have also

$$H_5 = b_5H_4, \tag{8}$$

where $b_5 = exp(i2k_0h)$. From Eqs. (5)–(8), we can obtain the H-field intensity of propagating wave 3

$$|H_3|^2 = C_r|H_1|^2, \tag{9}$$

where C_r is the evanescent-to-propagating wave conversion efficiency

$$C_r = 4\left|-\frac{b_2}{b_1} + \frac{(1+b_5)b_4}{(1-b_5)b_1} + \frac{b_4}{b_3}\right|^{-2}. \tag{10}$$

For narrow grooves ($\Delta \ll p$) and long wavelengths ($p \ll \lambda$ so that $k_{z1} \approx -ik_{x1}$ and $k_{z3} \approx k_0$), we have $b_1 \approx b_2 \approx 1$, $b_3 \approx ik_{x1}/(k_0f_s)$, and $b_4 \approx -f_s^{-1}$, where $f_s = \Delta/p$ is the filling ratio of the grooves. For frequencies near resonances (i.e. $2k_0h = (2m-1)\pi + \delta$ with m being a positive integer and $|\delta| \ll 1$, so that $(1+b_5)/(1-b_5) \approx -i\delta/2$), Eq. (10) can be approximately written as

$$C_r = \frac{4}{1 + 4Q^2(f/f_R - 1)}, \tag{11}$$

where the resonant frequency and Q-factor are given by

$$f_R = \frac{c(2m-1)}{4(h + f_s/k_{x1})},\ Q = \frac{(2m-1)\pi}{4f_s}. \tag{12}$$

The conversion efficiency C_r can reach its maximum 4 at resonant frequency, and become half maximum at frequency of $f_R(1 \pm Q/2)$. For the fundamental resonant mode with $m = 1$, we have

$$f_R = \frac{c}{4(h + f_s/k_{x1})},\ Q = \frac{\pi}{4f_s}. \tag{13}$$

In the above derivation, the incident evanescent wave 1 has a parallel wavenumber with $2\pi/p - k_0 \le k_{x1} \le 2\pi/p + k_0$, so that 1D spoof surface plasmon polaritons (SPPs) can be excited

OSA CONTINUUM

in the metal-groove metasurface. However, different from the previous cases with $|k_{x1}| \leq \pi/p$ [32,33], the spoof SPPs here possess larger parallel wavenumber, which can thus be folded above the light lines and exhibit radiation loss (i.e. propagating wave 3 is generated).

3. Results from theory and simulations

To verify the theory presented above, we conduct finite-element simulations for the metal-groove metasurfaces by using a commercial software (COMSOL MULTIPHYSICS) with finite-element method [22,23]. The metallic grooves are made of perfect electric conductor (PEC) and have a period $p = 60$ μm and depth $h = 0.8p$. The wave source is set to be either a downward evanescent wave or harmonic electric current source, which has a parallel wavenumber k_{x1} and frequency f and corresponds to swift charged particles with velocity of $v = pf$. The calculated frequency range will include the fundamental resonant frequency $f_R \approx c/4(h + f_s p/2\pi)$ of the metal-groove metasurface. We focus on the case of $k_{x1} = 2\pi/p$ where the wave 3 generated propagates along the z direction (i.e., $k_{x3} = 0$). It should be mentioned that all orders of the diffracted waves are included in the simulations. To obtain the amplitude of propagating wave 3, the Poynting vector needs to be calculated above the source [23].

Figure 2(a) shows the simulated evanescent-to-propagating wave conversion efficiency C_r for a metallic groove array with $f_s = 0.1$. We can see that the conversion efficiency exhibits a maximum of 3.88 at resonant frequency $f_R = 0.29c/p = 1.45$ THz. The corresponding Q-factor is 7.9, higher than that of Babinet metasurface (4.4). Such results are very close to those ($f_R = 0.306c/p = 1.53$ THz and $Q = 7.9$) from Eq. (10).

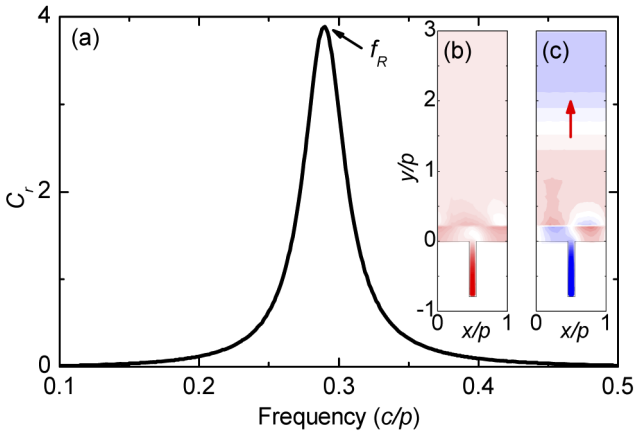

Fig. 2. (a) Conversion efficiency C_r as a function of frequency for the metal-groove metasurface in Fig. 1(a). The incident evanescent wave 1 has a parallel component of wavevector $k_{x1} = 2\pi/p$, and the outgoing propagating wave has a wavevector along the z direction (i.e., $k_{x3} = 0$). The metasurface is made of perfect electric conductor, and has parameters of $p = 60$ μm, $h = 0.8p$, and $\Delta = 0.1p$. The conversion efficiency has a maximum at resonant frequency f_R . (b) and (c) Distribution of $|H|$ and Re(H) at f_R in a unit cell of the metasurface, respectively. In (b), red and white colors relates to positive and zero values. In (c), red and blue colors corresponds to positive and negative values. The swift charged particles have parameters of $I_0 = 1$ A/m, $v = pf_R$, $z_0 = p/5$. The results are obtained by finite-element simulations.

The distribution of H-field in a unit cell is also calculated at resonant frequency, as shown in Figs. 2(b) and 2(c). Here, the swift charged particles are located at $z = 0.2p$. It can be seen that the amplitude of H-field exhibits local maxima at both the plane of moving charges ($z = z_0$) and the bottom of the metallic groove ($z = -h$) [Fig. 2(b)]. The depth of the metallic groove is about

OSA CONTINUUM

a quarter of the fundamental resonant wavelength. The Smith-Purcell radiation (i.e., wave 3) propagates indeed along the z direction [Fig. 2(c)].

On the basis of finite-element simulations, the spectra of conversion efficiency C_r are also been calculated for metasurfaces with different filling ratios of metal grooves [see Fig. 3]. We can see that for a large filling ratio ($f_s = 0.4$), the Q-factor is small ($Q = 2.07$), resulting in a moderate conversion efficiency ($C_{r,R} = 2.05$) at resonant frequency. As the filling ratio decreases ($f_s = 0.2$), a larger Q-factor is found ($Q = 4.06$), giving rise to a larger conversion efficiency ($C_{r,R} = 3.43$) at resonant frequency. But for filling ratios smaller than 0.1, the conversion efficiency remains almost constant ($C_{r,R} = 4$) although higher Q-factors are found. Such results are close to those from Eq. (10).

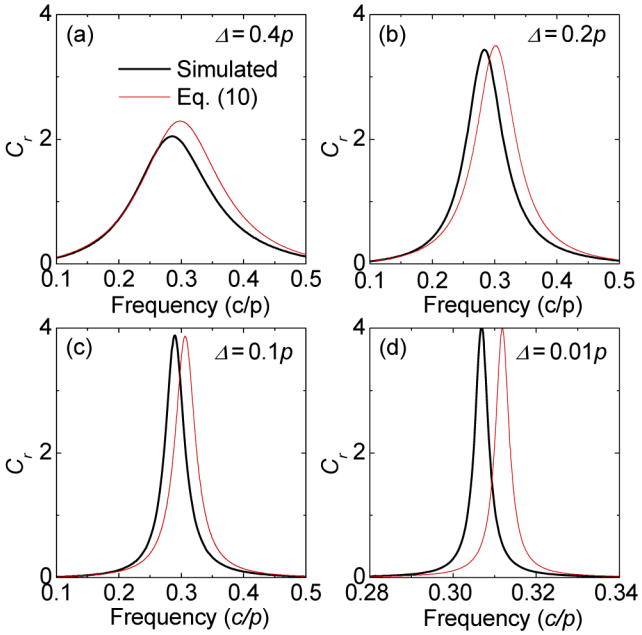

Fig. 3. Conversion efficiencies as a function of frequency for metal-groove metasurfaces with different groove width. (a) $\Delta = 0.4p$, (b) $\Delta = 0.2p$, (c) $\Delta = 0.1p$, and (d) $\Delta = 0.01p$. Other parameters are the same with those in Fig. 2(a). The black and red curves are obtained by finite-element simulations and Eq. (10), respectively.

Figure 4 illustrates the resonant frequency f_R, Q-factor, and evanescent-to-propagating wave conversion efficiency at f_R as a function of the filling ratio f_s of metal grooves. We can see that for wide metal grooves ($f_s > 0.3$), the resonant frequency decreases with decreasing the filling ratio of grooves [Fig. 4(a)]. But for narrow metal grooves ($f_s < 0.3$), the resonant frequency increases with decreasing the filling ratio of grooves and approaches to a constant ($f_R \approx c/4h$). In addition, the Q-factor is found to increase linearly with increasing $1/f_s$ [Fig. 4(b)]. However, the conversion efficiency $C_{r,R}$ at resonant frequency increases with decreasing the filling ratio f_s, but possesses an upper bound [$C_r < 4$, see Fig. 4(c)]. At f_s=0.05, the conversion efficiency $C_{r,R}$ is 3.97, very close to the upper bound of 4. Correspondingly, the conversion efficiency $C_{r,R}$ can increase with increasing the Q-factor, whereas it will be very close to the upper bound ($C_{r,max} = 4$) when $Q > 16$ (or $f_s < 0.05$). The simulated results and theoretical ones (from Eq. (10)) agree well with each other, and the discrepancies come from the neglect of high-order diffracted waves in the derivation of Eq. (10).

OSA CONTINUUM

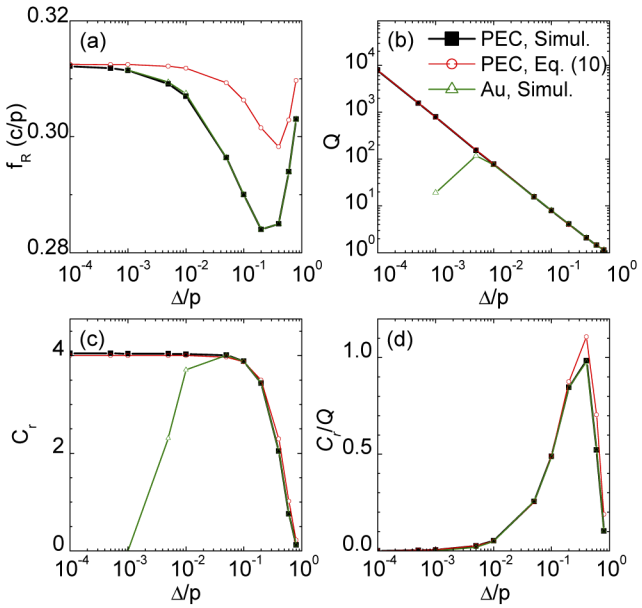

Fig. 4. (a) Resonant frequency f_R, (b) Q-factor, (c) conversion efficiency C_r at f_R and (d) C_r/Q as a function of the ratio of groove width to period. Other parameters are the same with those in Fig. 3. The black and red curves are for metal-groove metasurfaces made of perfect electric conductor, which are obtained by finite-element simulations and Eq. (10), respectively. The green curves are obtained by finite-element simulations for Au-groove metasurfaces with $p = 60$ μm. Other parameters are the same with those in Fig. 4.

The results presented above are for PEC groove arrays where absorption is neglected. We also simulate Au groove arrays with $p = 60$ μm and $h = 0.8p$ [see the green curves in Fig. 4]. Here, the dielectric constant of Au is described by a Drude model [34]. We can see that for wide Au grooves ($f_s > 0.005$), the Q-factor can increase with decreasing the filling ratio f_s of grooves [see Fig. 4(a)]. At an optimal filling ratio ($f_s = 0.005$), the Au groove array exhibits a maximal Q-factor ($Q_{\max} = 118$). Due to the existence of absorption, the Q-factor decreases with increasing the filling ratio fs for narrow Au grooves ($f_s < 0.005$). Similar change can also be seen for the conversion efficiency at resonant frequency [Fig. 4(b)]. However, the maximal conversion efficiency occurs in a relative large filling ratio ($f_s = 0.05$).

We note that both monochromaticity and output power are important indices of light sources. For free-electron light sources based on metasurfaces, monochromaticity is related to the Q-factor whereas the output power depends on a figure of merit $F \equiv C_r/Q$. For metal-groove metasurfaces with $f_s = 0.05$, a relatively high figure of merit ($F = 0.26$) can be obtained, much higher than the value ($F = 0.065$) in the recently reported double dielectric resonant gratings [26]. In fact, a higher figure of merit ($F = 0.98$) is available by using optimal filling ratio of grooves ($f_s = 0.4$) for the metal-groove metasurfaces ($C_r = 2.04$, $Q = 2.08$). The results indicate that metal-groove metasurfaces are good candidates for constructing high-power free-electron light sources.

4. Summary

In summary, we have presented a coupled mode theory to describe the Smith-Purcell radiation and evanescent-to-propagating wave conversion in metal groove metasurfaces. Analytic formulas are derived for the resonant frequency, Q-factor, and wave conversion efficiency at resonant frequency. The accuracy of the formulas is verified by finite-element simulations. It is found that

OSA CONTINUUM

for perfect-metal groove metasurfaces, the Q-factor can increase monotonically with decreasing the filling ratio of grooves. The conversion efficiency at resonant frequency can also increase with increasing the Q-factor, but exhibits an upper bound of 4. Such an upper limit of efficiency ($C_{r,max} = 4$) can be approached at a moderate Q-factor ($Q = 16$) or an optimal filling ratio of grooves ($f_s = 0.05$). Since the field is mainly located in the vacuum rather than the metallic part of the metasurfaces, the upper bound of efficiency can also be attained in practical Au-groove metasurfaces with absorption. Our results provides a comprehensive picture for the Smith-Purcell radiation in metal-groove metasurfaces and may benefit the construction of compact high-power free-electron light sources.

Funding

National Key Research and Development Program of China (2018YFA0306201); National Natural Science Foundation of China (11574037, 61422504).

Disclosures

The authors declare no conflicts of interest.

References

1. S. J. Smith and E. M. Purcell, "Visible light from localized surface charges moving across a grating," Phys. Rev. **92**(4), 1069 (1953).
2. P. A. Cerenkov, "Visible emission of clean liquids by action of gamma radiation," Dokl. Akad. Nauk SSSR **2**, 451 (1934).
3. P. M. van den Berg, "Smith-Purcell radiation from a line charge moving parallel to a reflection grating," J. Opt. Soc. Am. **63**(6), 689–698 (1973).
4. P. M. van den Berg, "Smith-Purcell radiation from a point charge moving parallel to a reflection grating," J. Opt. Soc. Am. **63**(12), 1588–1597 (1973).
5. L. Schachter and A. Ron, "Smith-Purcell free-electron laser," Phys. Rev. A **40**(2), 876–896 (1989).
6. K. Ishi, Y. Shibata, T. Takahashi, S. Hasebe, M. Ikezawa, K. Takami, T. Matsuyama, K. Kobayashi, and Y. Fujita, "Observation of coherent Smith-Purcell radiation from short-bunched electrons," Phys. Rev. E **51**(6), R5212–R5215 (1995).
7. K. J. Woods, J. E. Walsh, R. E. Stoner, H. G. Kirk, and R. C. Fernow, "Forward directed Smith-Purcell radiation from relativistic electrons," Phys. Rev. Lett. **74**(19), 3808–3811 (1995).
8. J. Urata, M. Goldstein, M. F. Kimmitt, A. Naumov, C. Platt, and J. E. Walsh, "Superradiant Smith-Purcell emission," Phys. Rev. Lett. **80**(3), 516–519 (1998).
9. S. E. Korbly and A. S. Kesar, "Observation of frequency-locked coherent terahertz Smith-Purcell radiation," Phys. Rev. Lett. **94**(5), 054803 (2005).
10. Y. Zhou, Y. Zhang, and S. Liu, "Electron-beam-driven enhanced terahertz coherent Smith-Purcell radiation within a cylindrical quasi-optical cavity," IEEE Trans. Terahertz Sci. Technol. **6**(2), 262–267 (2016).
11. N. Yu, P. Genevet, M. A. Kats, F. Aieta, J. P. Tetienne, F. Capasso, and Z. Gaburro, "Light propagation with phase discontinuities: generalized laws of reflection and refraction," Science **334**(6054), 333–337 (2011).
12. S. L. Sun, Q. He, S. Y. Xiao, Q. Xu, X. Li, and L. Zhou, "Gradient-index meta-surfaces as a bridge linking propagating waves and surface waves," Nat. Mater. **11**(5), 426–431 (2012).
13. N. Shitrit, I. Yulevich, E. Maguid, D. Ozeri, D. Veksler, V. Kleiner, and E. Hasman, "Spin-optical metamaterial route to spin-controlled photonics," Science **340**(6133), 724–726 (2013).
14. D. Lin, P. Fan, E. Hasman, and M. L. Brongersma, "Dielectric gradient metasurface optical elements," Science **345**(6194), 298–302 (2014).
15. G. Zheng, H. Muhlenbernd, M. Kenney, G. Li, T. Zentgraf, and S. Zhang, "Metasurface holograms reaching 80% efficiency," Nat. Nanotechnol. **10**(4), 308–312 (2015).
16. X. Li, L. Chen, Y. Li, X. Zhang, M. Pu, Z. Zhao, X. Ma, Y. Wang, M. Hong, and X. Luo, "Multicolor 3D meta-holography by broadband plasmonic modulation," Sci. Adv. **2**(11), e1601102 (2016).
17. S. Wang, P. C. Wu, V. C. Su, Y. C. Lai, C. H. Chu, J. W. Chen, S. H. Lu, J. Chen, B. Xu, C. H. Kuan, T. Li, S. Zhu, and D. P. Tsai, "Broadband achromatic optical metasurface devices," Nat. Commun. **8**(1), 187 (2017).
18. A. Tittl, A. Leitis, M. Liu, F. Yesilkoy, D. Y. Choi, D. N. Neshev, Y. S. Kivshar, and H. Altug, "Imaging-based molecular barcoding with pixelated dielectric metasurfaces," Science **360**(6393), 1105–1109 (2018).
19. G. Hu, X. Hong, K. Wang, J. Wu, H. Xu, W. Zhao, W. Liu, S. Zhang, F. Garcia-Vidal, B. Wang, P. Lu, and C. W. Qiu, "Coherent steering of nonlinear chiral valley photons with a synthetic Au–WS2 metasurface," Nat. Photonics **13**(7), 467–472 (2019).

OSA CONTINUUM

20. Z. Su, B. Xiong, Y. Xu, Z. Cai, J. Yin, R. Peng, and Y. Liu, "Manipulating Cherenkov Radiation and Smith–Purcell Radiation by Artificial Structures," Adv. Opt. Mater. **7**(14), 1801666 (2019).
21. T. Zhan, D. Han, X. Hu, X. Liu, S. T. Chui, and J. Zi, "Tunable terahertz radiation from graphene induced by moving electrons," Phys. Rev. B **89**(24), 245434 (2014).
22. Z. Wang, K. Yao, M. Chen, H. Chen, and Y. Liu, "Manipulating Smith-Purcell emission with Babinet metasurfaces," Phys. Rev. Lett. **117**(15), 157401 (2016).
23. L. Liu, H. Chang, C. Zhang, Y. Song, and X. Hu, "Terahertz and infrared Smith-Purcell radiation from Babinet metasurfaces: loss and efficiency," Phys. Rev. B **96**(16), 165435 (2017).
24. R. Remez, N. Shapira, C. Roques-Carmes, R. Tirole, Y. Yang, Y. Lereah, M. Soljacic, I. Kaminer, and A. Arie, "Spectral and spatial shaping of Smith-Purcell radiation," Phys. Rev. A **96**(6), 061801 (2017).
25. I. Kaminer, S. E. Kooi, R. Shiloh, B. Zhen, Y. Shen, J. J. Lopez, R. Remez, S. A. Skirlo, Y. Yang, J. D. Joannopoulos, A. Arie, and M. Soljacic, "Spectrally and spatially resolved Smith-Purcell radiation in plasmonic crystals with short-range disorder," Phys. Rev. X **7**(1), 011003 (2017).
26. Y. Song, N. Jiang, L. Liu, X. Hu, and J. Zi, "Cherenkov radiation from photonic bound states in the continuum: towards compact free-electron lasers," Phys. Rev. Appl. **10**(6), 064026 (2018).
27. Y. Ye, F. Liu, M. Wang, L. Tai, K. Cui, X. Feng, W. Zhang, and Y. Huang, "Deep-ultraviolet Smith–Purcell radiation," Optica **6**(5), 592–597 (2019).
28. Z. Su, F. Cheng, L. Li, and Y. Liu, "Complete control of Smith-Purcell radiation by graphene metasurfaces," ACS Photonics **6**(8), 1947–1954 (2019).
29. P. Zhang, L. Wang, Y. Zhang, A. Aimidula, and M. Tang, "Intensive vertical orientation Smith-Purcell radiation from the 2D well-array metasurface," Opt. Express **27**(4), 3952 (2019).
30. W. Liu and Z. Xu, "Special Smith-Purcell radiation from an open resonator array," New J. Phys. **16**(7), 073006 (2014).
31. Y. Song, J. Du, N. Jiang, L. Liu, and X. Hu, "Efficient terahertz and infrared Smith-Purcell radiation from metal-slot metasurfaces," Opt. Lett. **43**(16), 3858 (2018).
32. S. A. Maier, S. R. Andrews, L. Martin-Moreno, and F. J. Garcia-Vidal, "Terahertz surface plasmon-polariton propagation and focusing on periodically corrugated metal wires," Phys. Rev. Lett. **97**(17), 176805 (2006).
33. F. J. Garcia-Vidal, L. Martin-Moreno, and J. B. Pendry, "Surfaces with holes in them: new plasmonic metamaterials," J. Opt. A: Pure Appl. Opt. **7**(2), S97–S101 (2005).
34. M. A. Ordal, L. L. Long, R. J. Bell, S. E. Bell, R. R. Bell, R. W. Alexander Jr., and C. A. Ward, "Optical properties of the metals Al, Co, Cu, Au, Fe, Pb, Ni, Pd, Pt, Ag, Ti, and W in the infrared and far infrared," Appl. Opt. **22**(7), 1099 (1983).